Analysis of the total β-electron spectrum of ^{92}Rb: Implications for the reactor flux anomalies

M. Ramalho,[1,*] J. Suhonen,[1,†] J. Kostensalo,[2] G. A. Alcalá,[3] A. Algora,[3,4] M. Fallot,[5] A. Porta,[5] and A.-A. Zakari-Issoufou[5]

[1]*Department of Physics, University of Jyväskylä, P.O. Box 35, FI-40014, Jyväskylä, Finland*
[2]*Natural Resources Institute Finland, Yliopistokatu 6B, FI-80100 Joensuu, Finland*
[3]*Instituto de Física Corpuscular, CSIC-Universitat de València, E-46071 València, Spain*
[4]*Institute for Nuclear Research (Atomki), H-4001 Debrecen, Hungary*
[5]*SUBATECH, CNRS/IN2P3, IMT Atlantique, Nantes Université, F-44307 Nantes, France*

(Received 22 March 2022; accepted 1 August 2022; published 16 August 2022)

We present here a microscopic nuclear-structure calculation of a β-electron spectrum including all the β-decay branches of a high Q-value reactor fission product contributing significantly to the reactor antineutrino energy spectrum. We perform large-scale nuclear shell-model calculations of the total electron spectrum for the β^- decay of ^{92}Rb to states in ^{92}Sr using a computer cluster. We exploit the β-branching data of a recent total absorption γ-ray spectroscopy (TAGS) measurement to determine the effective values of the weak axial-vector coupling, $g_{\rm A}$, and the weak axial charge, $g_{\rm A}(\gamma_5)$. By using the TAGS data we avoid the bias stemming from the pandemonium effect which is a systematic error biasing the usual β-decay measurements. We take fully into account all the involved allowed and forbidden β transitions, in particular the first-forbidden nonunique ones which have earlier been shown to be relevant in the context of the reactor-antineutrino flux anomaly and the unexplained spectral shoulder, the "bump," the former one having been interpreted as one of the strongest evidence for the existence of sterile neutrinos. Here we are able to present quantitative evidence for the relevance of forbidden nonunique β^- decays in a total β spectrum of a fission product, in this case ^{92}Rb, which is one of the major contributors to the total reactor antineutrino spectral shape. We demonstrate that taking the forbidden spectral shapes fully into consideration leads for ^{92}Rb to a 2.6%–4.6% reduction in the expected inverse β-decay rate at the reactor antineutrino telescopes. We also confirm by our calculation of a total β-electron spectrum that the forbidden transitions can contribute to the formation of the spectral bump in the reactor-antineutrino flux profile.

DOI: 10.1103/PhysRevC.106.024315

I. INTRODUCTION

Neutrino-oscillation experiments and the subsequent analyses of their outcomes in the three-flavor framework have produced precision data on the mixing angles and magnitudes of the neutrino-mass splittings [1–3]. The three-flavor mixing framework was, however, challenged by the results of the reactor-antineutrino experiments RENO [4], Double Chooz [5], and Daya Bay [6]. When the measured antineutrino flux was compared with the predicted flux calculated using the standard Huber-Mueller (H-M) conversion method [7,8] based on the cumulative β-electron spectra measured by Schreckenbach *et al.* in the 1980s [9–12], two flux anomalies were recorded: a deficit of the measured flux relative to the predicted flux, coined the "reactor flux anomaly," or the "reactor antineutrino anomaly" (RAA) [13], and an unexpected spectral shoulder or "bump," an extra increase in the measured number of antineutrinos between 4 and 7 MeV of antineutrino energy. The significance of the RAA reaches up to 2.8σ [14] and depends on the adopted flux model [15]. The flux deficit has been hypothesized to be due to oscillations to a fourth neutrino flavor which does not interact with ordinary matter and is thus called a sterile neutrino. Sterile neutrinos have also been suggested as a potential solution to the so-called gallium anomaly [16], and such neutrinos are currently under a very active experimental search [17]. Furthermore, no explanation has been found for the spectral-bump anomaly within the H-M model.

An alternative to the H-M model is the summation method where all the individual beta branches are summed to produce the total β-electron spectrum nucleus by nucleus through the plethora of fission products of the reactor fuel. This model, originally proposed by King and Perkins [18] and further elaborated by others [19–22], is the only one able to access the various components of the total antineutrino flux and the related spectral shape. This method relies fully on the available nuclear data on fission yields, combined with the β-decay data on the fission products. The complications associated with the application of this method are the incompleteness of the nuclear data bases, their uncertainties, and systematic errors such as the pandemonium effect [23]. This effect is due to the limited efficiency of germanium detectors. Because γ-rays

*madeoliv@jyu.fi
†jouni.t.suhonen@jyu.fi

from high-energy nuclear levels may not be detected owing to efficiency issues, an underestimation of the β branchings to these states is produced. This, in turn, results in an overestimation of the high-energy part of the antineutrino spectrum in reactors.

The pandemonium effect can be circumvented in two ways: First, experimentally the weak β branches can be detected by total absorption γ-ray spectroscopy (TAGS), thus enabling the prediction of a more reliable antineutrino flux for the nuclear reactors. Hitherto, several TAGS measurement campaigns have led to numerous corrections to nuclear data regarding β-decay branches of relevant isotopes for the RAA [24–29]. Second, the correct β branchings could, in principle, be computed by using a suitable nuclear model, such as the nuclear shell model (NSM) with its several available Hamiltonians applicable to the key nuclei involved in the building of the total antineutrino flux. In this work we combine these two approaches and use the TAGS-measured branching data on the β decay of the 0^- ground state of ^{92}Rb to excited states in ^{92}Sr to guide our NSM calculations. The ^{92}Rb nucleus is one of the major contributors to the total antineutrino spectrum in nuclear reactors and the value of the important branching to the ^{92}Sr ground state has been independently verified by Rasco *et al.* [30]. We also compute the nuclear matrix elements (NMEs) involved in the forbidden nonunique β transitions, thus avoiding the previously used approximations where these transitions had been substituted by unique forbidden β transitions or allowed Gamow-Teller and Fermi transitions which all have universal β-electron spectral shapes. To our knowledge, the present work is the first one to venture a theoretical description of the total β-electron spectrum of a fission product with branchings to a large number of possible final states. Such a study gives important information on the contributions of the first-forbidden β decays to total β-electron spectra and eventually their importance in the reactor-antineutrino and bump anomalies.

The earlier studies such as the H-M model used allowed and forbidden unique β transitions as surrogates for forbidden nonunique β transitions, mostly due to computational difficulties. Doubts about the validity of this procedure were voiced by Hayes *et al.* [31] and Fang *et al.* [32]. In Hayen *et al.* [33,34] it was quantitatively shown by NSM calculations of key individual β transitions that the replacement of the nonunique β transitions by unique and allowed β transitions may lead to serious flaws in the estimations of the reactor antineutrino fluxes. This model, the "HKSS flux model" (coined as such by Berryman *et al.* [15]) has implications for both the RAA [15] and the spectral bump [33,34].

The first reasonable step in a full-blown nuclear-model analysis of the total antineutrino flux from nuclear reactors would be to try to compare the computed individual total β spectra with the TAGS-measured ones nucleus by nucleus. However, the corresponding nuclear-structure calculations face two specific complications: The first is related to the effective quenched value of the weak axial-vector coupling $g_{\rm A}^{\rm eff}$, and the second is related to the uncertain value of the weak axial charge $g_{\rm A}^{\rm eff}(\gamma_5)$, relevant for the first-forbidden nonunique β transitions without change in the nuclear angular momentum (i.e., the so-called $\Delta J = 0$ transitions). For more information on the values of these couplings and how they vary from nucleus to nucleus and β transition to β transition, see Refs. [35–39]). The electron spectral shapes have been found to be sometimes very sensitive to the value of $g_{\rm A}^{\rm eff}$ [38,40–45]. The weak axial charge $g_{\rm A}^{\rm eff}(\gamma_5)$, on the other hand, is enhanced by the meson-exchange currents [46–49] and the value of the related enhancement factor, $\varepsilon_{\rm MEC}$, as also its effects on β-electron spectra, has lately been systematically studied by Kostensalo *et al.* [39].

Since both $g_{\rm A}^{\rm eff}$ and $\varepsilon_{\rm MEC}$ possibly influence the β-electron spectra, a reasonable way to fix their values has to be found. In the present work we use the TAGS-measured branchings to groups of final states to determine the values of these two quantities. At the same time we keep an eye on the consistency with the systematics of Ref. [39] for $\varepsilon_{\rm MEC}$. For the vector part, as also for the allowed Fermi transitions, we adopt the conservation of vector current–protected (CVC-protected) value $g_{\rm V} = 1.0$ for the weak vector coupling.

The present article is organized as follows: First, in Sec. II, the adopted theoretical framework is briefly highlighted including a short introduction to the electron spectral shapes and an account of the involved shell-model calculations. We report and discuss the obtained results in Sec. III and draw conclusions in Sec. IV.

II. THEORETICAL FRAMEWORK

Here we describe briefly the theory framework used in the calculations, both the beta-decay formalism and the shell-model Hamiltonian.

A. Beta spectral shapes

The branching ratio of a transition to a particular final state in ^{92}Sr can be obtained from the corresponding partial half-life, which can be written as

$$t_{1/2} = \kappa/\tilde{C}, \tag{1}$$

where $\kappa = 6289$ s is a collection of natural constants [50] and the integrated shape function reads

$$\tilde{C} = \int_0^{w_0} C(w_e) p w_e (w_0 - w_e)^2 F_0(Z, w_e) dw_e. \tag{2}$$

In the above expression, $F_0(Z, w_e)$, with Z being the proton number of the daughter nucleus, is the usual Fermi function taking into account the final-state Coulomb distortion of the wave function of the emitted electron and $w_0 = W_0/m_e c^2$, $w_e = W_e/m_e c^2$, and $p = p_e c/m_e c^2 = (w_e^2 - 1)^{1/2}$ are kinematic quantities scaled dimensionless by the electron rest mass $m_e c^2$. Here p_e and W_e are the momentum and energy of the emitted electron, respectively, and W_0 is the beta endpoint energy, which for the ground-state transition defines the β-decay Q value. The shape factor is $C(w_e) \approx 1$ for allowed transitions [51] and it is quite a complicated combination of leptonic phase-space factors and NMEs, as described in detail in Ref. [52] and recently in Refs. [40,41].

In the present work, the needed β-decay formalism includes the allowed β decays (Fermi and Gamow-Teller) and the first-forbidden ones. The higher-forbidden β-decay

TABLE I. Level scheme of ^{92}Rb for the states with experimentally determined spin-parity. The known experimental states are compared with those computed using the two NSM Hamiltonians. The data were taken from Nuclear Data Sheets [55].

J^π	Expt. Energy (MeV)	*glepn* (MeV)	*glekpn* (MeV)
0^-	0.000	0.000	1.430
1^-	0.142	0.263	0.189
3^-	0.284	0.566	0.341

transitions are strongly suppressed and contribute a negligible amount to the summed electron spectral shape. The allowed decays are associated with a universal spectral shape, independent of the NMEs. This simple spectral shape, corresponding to $C(w_e) \approx 1$ in (2), has been extensively discussed in Ref. [51]. The first-forbidden β transitions are associated with tensor operators of rank 0 (0^-), 1 (1^-), and 2 (2^-) [36,37,52]. The pseudotensor 2^- transitions are pure axial-vector transitions and include only one NME and thus have a universal electron spectral shape. The pseudovector 1^- and pseudoscalar 0^- transitions have both vector and axial-vector components and depend on more than one NME, thus being sensitive to details of nuclear structure through the initial and final nuclear wave functions. For the vector part, as also for the allowed Fermi transitions, we adopt the CVC-protected value $g_{\rm V} = 1.0$ for the weak vector coupling. The pseudoscalar 0^- transitions are pure axial vector and depend on the weak axial charge $g_{\rm A}(\gamma_5)$, in addition to $g_{\rm A}$. These are the $\Delta J = 0$ transitions and their decay rate depends on the value of the enhancement factor $\varepsilon_{\rm MEC}$, multiplying the $g_{\rm A}(\gamma_5)$ term. Again, more than one NME is involved so that these transitions are nuclear-structure sensitive. Since in the present case the initial state of β decay is 0^-, the pseudoscalar transitions go to 0^+ states, the pseudovector transitions to 1^+ states and the pseudotensor transitions to 2^+ states. Here it should be noted that, for initial states with nonzero angular momentum, the situation is more complicated and more than one of these transition types may contribute for a given final state, with interesting consequences, as demonstrated in Refs. [33,34].

B. Shell-model calculations

The NSM calculations were performed using the software NUSHELLX@MSU [53]. The interactions used in this work were *glekpn* and *glepn*, all originally designed to access the spectroscopy of ^{96}Y and ^{96}Zr in Ref. [54]. Thus, the single-particle energies were fit to a nuclear region suitable for the present studies. The single-particle model space for *glekpn* consists of the proton orbitals $1f_{5/2}$, $2p_{3/2}$, $2p_{1/2}$, and $1g_{9/2}$, with $1f_{7/2}$ as a closed shell, and the neutron orbitals $1g_{7/2}$, $2d_{5/2}$, $2d_{3/2}$, and $3s_{1/2}$, with $1g_{9/2}$ as a closed shell. The *glepn* has the single-particle model space with the proton orbitals $2p_{3/2}$, $1f_{5/2}$, $2p_{1/2}$, $1g_{9/2}$, and $3s_{1/2}$ while for neutrons all shells up to $1g_{9/2}$ are filled and the orbitals $3s_{1/2}$, $2d_{5/2}$, and $2d_{3/2}$ form the valence space. This setup enabled us to compute the level energies of ^{92}Rb (see Table I) and ^{92}Sr (see Table II). For ^{92}Rb only the lowest three states have an unambiguously assigned spin-parity. The corresponding *glepn*-computed and *glekpn*-computed states are given for comparison in Table I. Notably, the *glepn* interaction reproduces quite nicely the energies of the corresponding experimental states, but for *glekpn* the 0^- state is quite high in energy and the ground state is a 2^- state. This is not unusual for typical shell-model Hamiltonians trying to predict state energies in odd-odd nuclei. In these nuclei one has to cope with an extremely high density of states so that prediction of a correct level sequence is more luck than a general rule. In the experimental spectrum there are a lot of states, above those listed in the table, with the ambiguous spin-parity assignment "$(1, 2^-)$." Also, in both computed spectra there are a lot of 1^-, 2^-, and 3^- states at low energies. As can be seen in Table II, the level scheme of ^{92}Sr could be reproduced within a few hundreds of keV accuracy. For ^{92}Sr, both interactions manage to predict the correct level sequence, which is easier than for ^{92}Rb since the state density in an even-even nucleus is much less than in an odd-odd one.

TABLE II. Clustering of states of ^{92}Sr for the determination of possible values of the pair $[g_{\rm A}^{\rm eff}, \varepsilon_{\rm MEC}]$. Parentheses indicate uncertainty in parity and/or angular momentum. The columns *glekpn* and *glepn* are the adopted interactions and their corresponding predicted energy schemes. Superscript numbers above each interaction's level schemes indicates the cluster in which the corresponding state has been assigned in determination of the pairs. The experimental level energies of ^{92}Sr were taken from Nuclear Data Sheets [55].

Energy (keV)	J^π	*glekpn*	*glepn*
0.0	0^+	0^1	0^1
814.98	2^+	1102^2	848^2
1384.79	2^+	1926^2	1793^2
1778.33	$2^{(+)}$	2341	2074^2
2053.9	(2^+)		2347
2088.39	$0^{(+)}$		
2140.82	1^+	2405^2	2552^2
2765.7	0^+	2863^2	2924
2783.6	$[2^+]$[a]	2974	3011
2820.89	$([2^+], 1)$[b]	3513^2	3437^2

[a]State predicted by both interactions but of experimentally unknown parity and spin.
[b]Square brackets denote interactions' spin-parity prediction.

After the level schemes were produced for both NSM interactions, the β^--decay transitions from the 0^- ground state of ^{92}Rb to the 0^+, 1^+, 2^+, and 1^- states in ^{92}Sr were computed for further studies of the β feeding of ^{92}Sr. For the ground-state-to-ground-state decay energy we adopted the experimental value $Q = 8.095$ MeV.

III. RESULTS

Here we describe the flow of the calculations and the subsequent analyses. The predicted decay branchings, partial half-lives, and electron spectral shapes are dependent on the available endpoint energies (equal to the Q value for the ground-state transition, taken from experiment in the present work) and the values of $g_{\rm A}^{\rm eff}$ and $\varepsilon_{\rm MEC}$ (the latter for $\Delta J = 0$ transitions). This means that a reasonable theoretical description of all these aspects is a demanding task, and we have

chosen to tackle the related problems in a way described in the following.

A. Determination of the values of the axial couplings

Our assessment of the values of g_A^{eff} and ε_{MEC} utilizes the TAGS-measured branching data by suitably clustering the final states in ^{92}Sr. This clustering includes the strong transition to the ground state as cluster number 1 and cluster 2 includes transitions to several excited states, as shown in Table II for each of the interactions used in the present calculations. All final states in the table correspond to first-forbidden transitions. Concerning the *glekpn* interaction, the 2^+ states at energies 1384.79 and 1778.33 keV were a bit problematic since excessively large branchings to these states were predicted by the calculations. We then opted for the 0^+ states at 2088.39 and 2527.18 keV to be used for determination of the values of the weak couplings for this interaction. Such differences between the results obtained by using the two shell-model Hamiltonians are not so surprising considering their different valence spaces, single-particle energies, and effective two-body interaction matrix elements. While it is true that selecting different final states in group 2 for the two interactions biases the choice of values of the weak couplings g_A^{eff} and ε_{MEC}, resulting in two different sets of these parameters, this only implies that the different Hamiltonians used in the calculations necessitate different effective values of these weak couplings.

Since all the individual branchings in cluster 2 are small and thus liable to large relative errors, we chose to sum up all the individual branchings to produce a larger summed branching which is easier to compare with the corresponding sum of the computed branchings. This procedure dampens the variations in the computed individual branchings among the two interactions used in the calculations. Since the branching corresponding to the ground-state-to-ground-state transition is large and best known we set a criterion of 2.5% relative error for the corresponding computed branching. For cluster 2 we adopted a less restrictive criterion of 25% relative error in the computed sum branching. We then searched for values of $[g_A^{\text{eff}}, \varepsilon_{\text{MEC}}]$ pairs satisfying both of the mentioned criteria by varying g_A^{eff} within the range from 0.2 to 1.27 and ε_{MEC} in the range between 0.7 and 2.0. In all these calculations we use the experimentally known excitation energies of the involved final states in order to treat correctly the lepton phase space with an accurate endpoint energy.

The obtained values of the pair were found to follow a regular pattern for each interaction. The patterns are reproduced by the polynomial regressions

$$\varepsilon_{\text{MEC}} = 0.572(4)g_A^2 - 1.755(3)g_A + 2.539(9), \quad (3)$$

$$\varepsilon_{\text{MEC}} = 1.003(2)g_A^2 - 2.948(4)g_A + 3.582(8), \quad (4)$$

for *glekpn* and *glepn*, respectively. For the former, it correctly predicts the pattern in the range $g_A^{\text{eff}} = 0.76$–1.27 and the latter $g_A^{\text{eff}} = 0.70$–1.27. Lastly, from the pool of solutions we picked one $[g_A^{\text{eff}}, \varepsilon_{\text{MEC}}]$ combination for each interaction with the least relative branching error, below or equal to 0.25%, for the ground-state-to-ground-state decay branch. The obtained $[g_A^{\text{eff}}, \varepsilon_{\text{MEC}}]$ combinations were [1.106, 1.3] and [1.083, 1.57] for *glekpn* and *glepn*, respectively. The corresponding range, $\varepsilon_{\text{MEC}} = 1.3$–$1.6$, for the mesonic enhancement factor is compatible with that found for the corresponding mass region in Ref. [39] for values $g_A^{\text{eff}} = 0.7$–1.0. Here it has to be pointed out that the presently obtained range $g_A^{\text{eff}} \approx 1.0$–$1.1$ does not represent only the $0^- \to 0^+$ transition but also transitions to 1^+ and 2^+ states, contrary to the analysis in Ref. [39]. Furthermore, the solutions in the lower and upper limits of g_A^{eff} introduce variations from the selected solution's total branching ranging from a minimum 0.7% to a maximum of 3.8%. The effects on the total spectral shape by these variations are quite small, and in the reasonable physical range $g_A^{\text{eff}} = 0.9$–1.2 even negligible. Due to this insensitivity to a reasonable variation in the values of the axial couplings and the fact that the major player in the parameter determination, the ground-state transition, has small experimental error bars in its measured branching, the experimental error bars in the measured branchings of groups 1 and 2 have a negligible impact on the computed spectral shapes. This indicates that our results concerning the total electron spectral shape are quite robust.

B. Computation of the electron spectral shapes

With the selected combinations of the weak couplings we can proceed with our calculations of the NMEs and their corresponding half-lives and electron spectra. We include in the calculations all allowed and first-forbidden transitions but leave out the higher-forbidden ones due to their strong hindrance and negligible contribution. Most of the final states within the Q window have not been included in the fitting procedure. The allowed Fermi and Gamow-Teller decays to the 0^- and 1^- states have a universal electron spectral shape and can thus be treated exactly by using the TAGS-measured branchings, thus minimizing the computational error related to these decays.

The first-forbidden transitions, beyond the states included in cluster 2, pose a source of uncertainty in our calculations as their precise state energies are experimentally unresolved, leading to uncertainties in the associated endpoint energies, branchings, and therefore their electron spectral shapes. The related error can be analyzed via comparison of the TAGS-measured total branching ratio and the corresponding computed one for transitions to the energy region containing the unresolved states.

Additionally, one can check the robustness of the spectral-shape prediction by adding (removing) a uniform amount of 250 keV to (from) the computed endpoint energies of the unresolved states. These shifts are reasonable considering the uncertainties in the level energies of the known states in groups 1 and 2, but this is just a nomenclature and does not mean that all the levels should shift uniformly, but rather in random, in any realistic scenario. By this nomenclature of uniform shifts we want to produce the maximal impact on the computed spectral shapes to see how robust our predictions are in this respect. The related effects are shown in Fig. 1 for the *glekpn* interaction where, for convenience, the area under the curves is normalized to unity to produce the same total half-life for each case. From the lower panel of the figure one

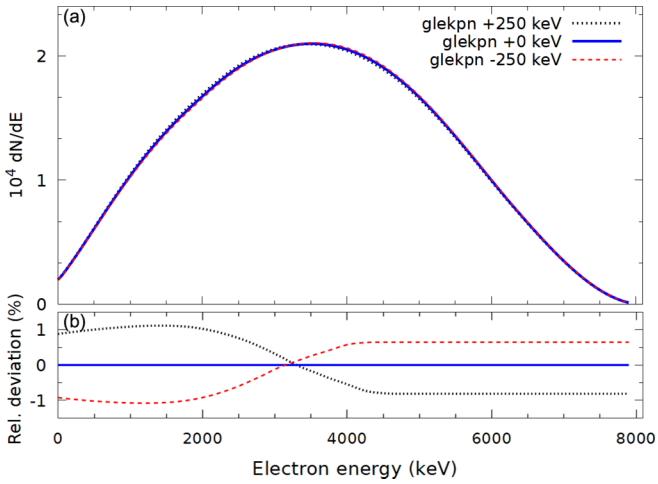

FIG. 1. (a) Analysis of the effects of uniformly over- or under-predicting by 250 keV (the dotted and dashed lines, respectively) the *glekpn*-computed endpoint energies (solid line) of the unresolved states. The horizontal axis indicates the electron kinetic energy and the vertical axis is given in arbitrary units such that the total area under the curves is normalized to unity (upper panel). (b) Plot of the relative deviation in percent. The semistraight lines after 4000 keV are due to the normalization to unity.

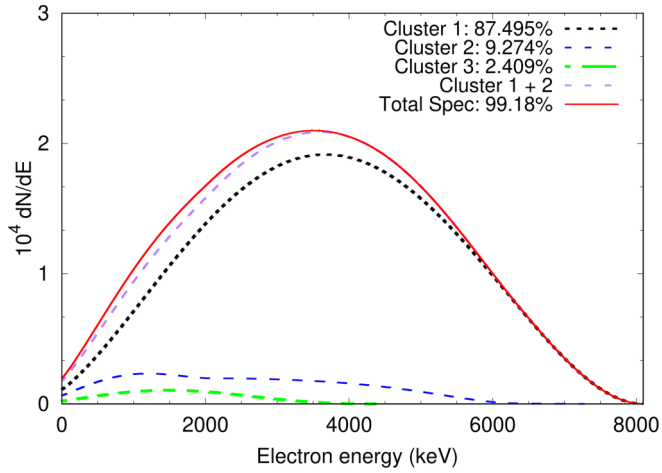

FIG. 2. The *glekpn*-computed total spectrum and its decomposition into contributions from the ground-state transition (cluster 1), the known forbidden (cluster 2) plus allowed transitions and the unresolved transitions (cluster 3). The cluster build-up to the total spectrum (clusters 1,2 and 3 combined) is also shown.

can see that the effects of these shifts are at a sub-percent level indicating that the unresolved states do not contribute significantly to the total spectral shape. The same is true for the *glepn* interaction. The related robust theory description can be seen from the variation of the total branching ratio to the unresolved states which now becomes $2.40^{+0.82}_{-0.63}\%$ and $2.26^{+0.70}_{-0.55}\%$ for *glekpn* and *glepn*, respectively, in good agreement with the TAGS-measured branching $2.81^{+1.32}_{-0.98}\%$.

C. Total electron spectral shape

After all these procedures and checks of robustness, we are ready to proceed to combine the calculated NMEs and phase-space factors into electron spectral shapes. In Fig. 2 we show the decomposition of the total electron spectral shape, again for the *glekpn* interaction. It can be seen that the dominant component is the first-forbidden nonunique decay to the ground state (cluster 1) and then come the first-forbidden of cluster 2 plus allowed transitions, with known experiment-based Q values. The smallest contribution comes from cluster 3, containing the rest of the states, including the unresolved first-forbidden transitions. The small contribution of the states in cluster 3 is clearly seen as the difference between the cumulative curves with solid line (total spectrum) and dotted line (total minus cluster 3), the deviations showing up below some 3.5 MeV of electron kinetic energy. For the *glepn* interaction a similar pattern is recorded. The percentages shown in the figure are the computed contributions to the measured total half-life. Since our calculations only include transitions to states of spins 0, 1, and 2, leaving out the higher-forbidden transitions, our calculations underpredict the total half-life by the missing 0.82%.

As a final step, we compare the computed total sum spectra with the one obtained from a simulation employing the ^{92}Rb beta branchings from the TAGS measurements. In the TAGS spectrum, we exclusively use allowed shapes for all transitions from the parent ground state to the lowest and highest discrete and (continuum-like) high-density daughter energy states, respectively. The Fermi function correction based on Evans [56] was added to all transitions. This comparison is depicted in Fig. 3, where the TAGS result is denoted the "TAS" Spectrum. The area under each curve is the same since the same total half-life was obtained for each case. For convenience, this area is normalized to one in the figure. The lower panel of the figure gives the relative deviation of the curves in percent. We have tested that switching all the NSM-computed spectral

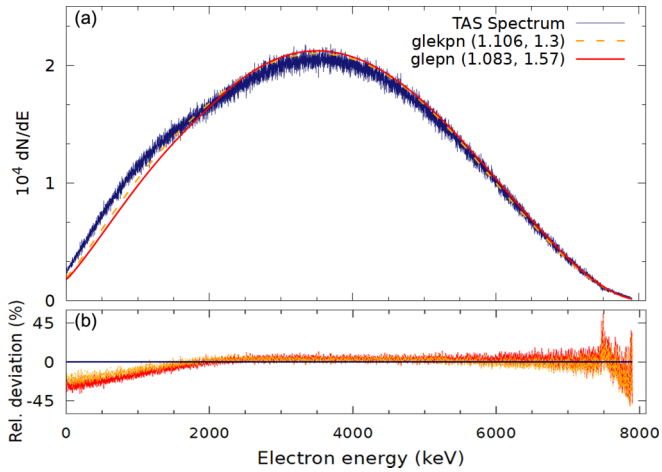

FIG. 3. (a) Comparison of the simulated TAGS total beta spectrum (thick fuzzy line) with those computed by using the shell-model interactions *glekpn* (dashed curve) and *glepn* (line). The horizontal axis indicates the electron kinetic energy and the vertical axis is given in arbitrary units such that the total area under the curves is normalized to unity. (b) Relative deviation in percent of the computed spectral curves (fuzzy line) from the simulated TAGS curve.

shapes allowed, i.e., making the "all-allowed" approximation in the total NSM-computed spectral shape reproduces the "TAS spectrum" of Fig. 3. Both the simulated TAGS spectrum and the all-allowed NSM spectrum are based on the TAGS-measured branchings, so that their coincidence can be used as a check of the consistency of the NSM calculations. It can be seen that abandoning the allowed approximation for the first-forbidden decay transitions of clusters 1 and 2, makes a clear difference, and the spectral shape changes in a similar way relative to the allowed approximation for the two interactions. The main differences are at low electron kinetic energies, below 2 MeV, where the interactions predict a clear deficit in the number of electrons, and in intermediate energies, between 2 and 4 MeV, where the interactions predict a slight excess of electrons.

The shell-model calculations predict a smaller number of low energy electrons than the TAGS analysis based on allowed transitions. This would mean less higher energy antineutrinos, which can have an outsized effect on the number of detected antineutrinos in antineutrino telescopes, since the cross section is roughly proportional to $E_e p_e$ [57], where E_e is the energy and p_e the momentum of the produced positron. Simulating the NSM-based and TAGS-based antineutrino spectra we found that the expected inverse beta decay (IBD) rate is 2.6% smaller for the *glekpn*-based and 4.6% smaller for the *glepn*-based antineutrino spectrum than for the TAGS-based one. While these results indicate that the allowed approximation leads to an over estimation of a couple of percent in the IBD rate they most importantly demonstrate the uncertainties related to the prediction of IBD rates for antineutrinos from fission fragments relevant for the reactor-flux anomalies. Furthermore, our "by-the-eye" analyses indicate that taking fully into account the first-forbidden β transitions leads in the case of the ^{92}Rb decay to a flux deficit at antineutrino energies above 6 MeV and to a flux excess in the energy interval 4–6 MeV. Thus ^{92}Rb could be conjectured to contribute to the emergence of the spectral bump in the reactor-antineutrino flux. Making this a bit more quantitative, we can use the fission yield 4.8% of ^{92}Rb and our computed reduction of 2.6%–4.6% in the IBD rate to produce an estimated reduction of 0.13%–0.22% in the total reactor-antineutrino flux by ^{92}Rb alone. This means that only a more comprehensive analysis, including a number of other nuclei contributing to the antineutrino flux, can verify quantitatively the impact of the first-forbidden transitions to the RAA and the spectral bump.

IV. CONCLUSIONS

In this work we report on the first computation of the shape of a total electron spectrum related to beta-decay transitions to final states within a full decay Q window. Specifically, we calculate the total electron spectral shape related the β^- transitions from the 0^- ground state of ^{92}Rb to excited states in ^{92}Sr within the full Q window of 8.095 MeV. All relevant allowed and first-forbidden beta transitions are included and data on measured excitation energies of the final states and the TAGS-measured beta branching ratios are used as guidelines to adjust the values of the involved weak axial-vector and axial-charge couplings. Ultimately, these type of calculations for the most important fission products in nuclear reactors will pave the way to a better understanding of the reactor antineutrino spectra and the related flux and bump anomalies. By calculating the total electron spectral shape we have been able to demonstrate in a robust way that the first-forbidden β^- transitions can significantly affect this shape for a given fission product, in this case for ^{92}Rb, a major contributor to the reactor-antineutrino spectral shape. These corrections were shown to lead to a decrease of 2.6%–4.6% in the expected IBD rate thus demonstrating the percent-scale impact on the predicted antineutrino detection rates in antineutrino telescopes. We could also show that the decay of ^{92}Rb potentially contributes to the RAA by some 0.13%–0.22% reduction in the flux. Furthermore, "by-the-eye" inspection shows qualitatively that ^{92}Rb could contribute to the formation of the bump in the reactor-antineutrino flux profile. This said, one has to keep in mind that ^{92}Rb is only one of the so many fission products contributing to the total antineutrino flux from reactors. Based on the decay study of this one sole nucleus it is hard to make quantitative conclusions about the impact of the forbidden β transitions on the total antineutrino spectrum. Here one would need to proceed step by step, treating the most prominent flux contributors ^{90}Rb, ^{94}Y, ^{96}Y, ^{140}Xe, ^{140}Cs, . . ., one after another, as also suggested in Ref. [58]. This we leave for future work.

ACKNOWLEDGMENTS

We acknowledge the support by the Academy of Finland under the Contract No. 318043 and grants for computer resources from the Finnish Grid and Cloud Infrastructure (persistent identifier urnnbnfiresearch-infras-2016072533). Colleagues from SUBATECH and Spain would like to thank the Master Projects TAGS, Jyvaskyla and OPALE from CNRS/in2p3, the CNRS IRN ASTRANUCAP, the NEEDS/NACRE project, the CHANDA and SANDA European projectS, the University of Nantes, and the region Pays de Loire for their contributions to the funding of the TAGS experiments.

[1] P. De Salas, D. Forero, M. Tórtola, and J. Valle, Phys. Lett. B **782**, 633 (2018).

[2] F. Capozzi, E. Lisi, A. Marrone, and A. Palazzo, Prog. Part. Nucl. Phys. **102**, 48 (2018).

[3] I. Esteban, M. C. Gonzalez-Garcia, A. Hernandez-Cebezudo, M. Maltoni, and T. Schwetz, J. High Energy Phys. 01 (2019) 106.

[4] J. K. Ahn *et al.* (RENO Collaboration), Phys. Rev. Lett. **108**, 191802 (2012).

[5] Y. Abe *et al.* (Double Chooz Collaboration), J. High Energy Phys. 10 (2014) 086.
[6] B. Pal *et al.* (Daya Bay Collaboration), Phys. Rev. Lett. **116**, 161801 (2016).
[7] P. Huber, Phys. Rev. C **84**, 024617 (2011).
[8] T. A. Mueller *et al.*, Phys. Rev. C **83**, 054615 (2011).
[9] K. Schreckenbach, H. R. Faust, F. von Feilitzsch, A. A. Hahn, K. Hawerkamp, and J. L. Vuilleumier, Phys. Lett. B **99**, 251 (1981).
[10] F. von Feilitzsch, A. A. Hahn, and K. Schreckenbach, Phys. Lett. B **118**, 162 (1982).
[11] K. Schreckenbach, G. Colvin, W. Gelletly, and F. von Feilitzsch, Phys. Lett. B **160**, 325 (1985).
[12] A. A. Hahn, K. Schreckenbach, W. Gelletly, F. von Feilitzsch, G. Colvin, and B. Krusche, Phys. Lett. B **218**, 365 (1989).
[13] G. Mention, M. Fechner, T. Lasserre, T. A. Mueller, D. Lhuillier, M. Cribier, and A. Letourneau, Phys. Rev. D **83**, 073006 (2011).
[14] S. Gariazzo, C. Giunti, M. Laveder, and Y. F. Li, J. High Energy Phys. 06 (2017) 135.
[15] J. M. Berryman and P. Huber, Phys. Rev. D **101**, 015008 (2020).
[16] J. Kostensalo, J. Suhonen, C. Giunti, and P. C. Srivastava, Phys. Lett. B **795**, 542 (2019).
[17] S. Schoppmann, Universe **7**, 360 (2021).
[18] R. W. King and J. F. Perkins, Phys. Rev. **112**, 963 (1958).
[19] F. T. Avignone, S. M. Blakenship, and C. W. Darden, Phys. Rev. **170**, 931 (1968).
[20] P. Vogel, G. K. Schenter, F. M. Mann, and R. E. Schenter, Phys. Rev. C **24**, 1543 (1981).
[21] O. Tengblad, K. Aleklett, R. Von Dincklage, E. Lund, G. Nyman, and G. Rudstam, Nucl. Phys. A **503**, 136 (1989).
[22] G. Rudstam, P. I. Johansson, O. Tengblad, P. Aagaard, and J. Eriksen, At. Data Nucl. Data Tables **45**, 239 (1990).
[23] J. C. Hardy, L. C. Carraz, B. Jonson, and P. G. Hansen, Phys. Lett. B **71**, 307 (1977).
[24] A. Algora *et al.*, Phys. Rev. Lett. **105**, 202501 (2010).
[25] M. Fallot *et al.*, Phys. Rev. Lett. **109**, 202504 (2012).
[26] A. A. Zakari-Issoufou, M. Fallot, A. Porta, A. Algora, J. L. Tain, E. Valencia, S. Rice, V. Bui, S. Cormon, M. Estienne, J. Agramunt, J. Aysto, M. Bowry, J. A. Briz, R. Caballero-Folch, D. Cano-Ott, A. Cucoanes, V. V. Elomaa, T. Eronen, E. Estevez, G. F. Farrelly, A. R. Garcia, W. Gelletly, M. B. Gomez-Hornillos, V. Gorlychev, J. Hakala, A. Jokinen, M. D. Jordan, A. Kankainen, P. Karvonen, V. S. Kolhinen, F. G. Kondev, T. Martinez, E. Mendoza, F. Molina, I. Moore, A. B. Perez-Cerdan, Z. Podolyak, H. Penttila, P. H. Regan, M. Reponen, J. Rissanen, B. Rubio, T. Shiba, A. A. Sonzogni, and C. Weber (IGISOL Collaboration), Phys. Rev. Lett. **115**, 102503 (2015).
[27] E. Valencia *et al.*, Phys. Rev. C **95**, 024320 (2017).
[28] S. Rice *et al.*, Phys. Rev. C **96**, 014320 (2017).
[29] V. Guadilla *et al.*, Phys. Rev. Lett. **122**, 042502 (2019).
[30] B. C. Rasco *et al.*, Phys. Rev. Lett. **117**, 092501 (2016).
[31] A. C. Hayes, J. L. Friar, G. T. Garvey, G. Jungman, and G. Jonkmans, Phys. Rev. Lett. **112**, 202501 (2014).
[32] D. L. Fang and B. A. Brown, Phys. Rev. C **91**, 025503 (2015).
[33] L. Hayen, J. Kostensalo, N. Severijns, and J. Suhonen, Phys. Rev. C **99**, 031301(R) (2019).
[34] L. Hayen, J. Kostensalo, N. Severijns, and J. Suhonen, Phys. Rev. C **100**, 054323 (2019).
[35] J. Engel and J. Menéndez, Rep. Prog. Phys. **80**, 046301 (2017)
[36] J. T. Suhonen, Front. Phys. **5**, 55 (2017).
[37] H. Ejiri, J. Suhonen, and K. Zuber, Phys. Rep. **797**, 1 (2019).
[38] J. Suhonen and J. Kostensalo, Front. Phys. **7**, 29 (2019).
[39] J. Kostensalo and J. Suhonen, Phys. Lett. B **781**, 480 (2018).
[40] M. Haaranen, P. C. Srivastava, and J. Suhonen, Phys. Rev. C **93**, 034308 (2016).
[41] M. Haaranen, J. Kotila, and J. Suhonen, Phys. Rev. C **95**, 024327 (2017).
[42] J. Kostensalo, M. Haaranen, and J. Suhonen, Phys. Rev. C **95**, 044313 (2017).
[43] J. Kostensalo and J. Suhonen, Phys. Rev. C **96**, 024317 (2017).
[44] L. Bodenstein-Dresler *et al.* (COBRA Collaboration), Phys. Lett. B **800**, 135092 (2020).
[45] J. Kostensalo, J. Suhonen, J. Volkmer, S. Zatschler, and K. Zuber, Phys. Lett. B **822**, 136652 (2021).
[46] K. Kubodera, J. Delorme, and M. Rho, Phys. Rev. Lett. **40**, 755 (1978).
[47] J. Delorme, Nucl. Phys. A **374**, 541 (1982).
[48] E. K. Warburton, Phys. Rev. C **44**, 233 (1991).
[49] K. Kubodera and M. Rho, Phys. Rev. Lett. **67**, 3479 (1991).
[50] A. Kumar, P. C. Srivastava, and J. Suhonen, Eur. Phys. J. A **57**, 225 (2021).
[51] J. Suhonen, *From Nucleons to Nucleus: Concepts of Microscopic Nuclear Theory* (Springer-Verlag, Berlin, Heidelberg, Springer, Gaithersburg, 20899, 2007).
[52] H. Behrens and W. Bühring, *Electron Radial Wave Functions and Nuclear Beta-decay (International Series of Monographs on Physics)* (Clarendon Press, Oxford, 1982).
[53] B. A. Brown and W. D. M. Rae, Nucl. Data Sheets **120**, 115 (2014).
[54] H. Mach, E. K. Warburton *et al.*, Phys. Rev. C **41**, 226 (1990).
[55] C. M. Baglin, Nucl. Data Sheets **113**, 2187 (2012).
[56] R. Evans, *The Atomic Nucleus* (McGraw-Hill Publishing Company, Ltd., 1955).
[57] A. C. Hayes and P. Vogel, Annu. Rev. Nucl. Part. Sci. **66**, 219 (2016).
[58] A. A. Sonzogni, T. D. Johnson, and E. A. McCutchan, Phys. Rev. C **91**, 011301(R) (2015).